

Star formation at high redshift as traced by near-infrared H α emission surveys

Paul P. van der Werf
Leiden Observatory, The Netherlands.



Abstract

Surveys of redshifted emission lines in the near-infrared will provide unique information on the cosmic star formation history. Near-infrared H α surveys will probe the cosmic star formation density and the evolution of the luminosity function of star forming galaxies out to $z \sim 2.5$, including the important $z = 1.5 - 2.0$ epoch, where according to current knowledge the cosmic star formation density peaks. H α and other hydrogen recombination lines (except Ly α) and [O II] are all useful tracers of star formation provided the luminosity function is probed to sufficiently deep levels. However, shallow surveys or surveys of Ly α or [O III] emission are not suitable for measuring or even constraining the cosmic star formation density. A first estimate of the star formation density at $z \approx 2.25$ is derived, based on a new and sensitive large-area ESO near-infrared survey for H α emission at this redshift. Future observational directions, at near-infrared and longer wavelengths, for reading the cosmic star formation history are outlined.

1 Introduction

The very rapid developments in near-infrared (near-IR) array technology of the last few years have brought about a revolution in the field of emission line surveys in the near-IR wavebands. Until recently such surveys did not yield any detections [30, 20, 2], although these null-results in some cases began to set interesting limits on the number density of the most luminous emission line galaxies [31]. The recent availability of near-IR cameras with large-format arrays has now produced the first detections in surveys for H α emission at high redshift. While the number of

Invited Review to appear in “*Extragalactic Astronomy in the Infrared*”, eds. G. A. Mamon, Trinh Xuân Thuận, & J. Trân Thanh Vân, Editions Frontières, Gif-sur-Yvette

detections is still small, this result for the first time provides a crude estimate of the density of luminous emission line objects at cosmological distances. Simultaneously, a change of focus has taken place. Whereas previously surveys were aimed at finding only the most luminous objects, current technology allows deeper searches, and for the first time an estimate of the star formation density (SFD) at $z \approx 2.25$ is obtained. Future surveys will be able to probe the luminosity function to even greater depth.

This review first discusses our current state of knowledge of the star formation history of the universe, and the crucial role which near-IR emission line surveys will play in this field (Sect. 2). Subsequently the use (and limitations) of emission lines as cosmic star formation tracers is discussed (Sect. 3). Then, results of the ESO near-IR H α survey are presented, and implications for the cosmic SFD at $z \approx 2.25$ are derived (Sect. 4). Finally, prospects for future observational work, using H α and other tracers, for tracing the star formation history of the universe are discussed (Sect. 5). Throughout this paper the Hubble constant is written as $H_0 = 75 h_{75} \text{ km s}^{-1} \text{ Mpc}^{-1}$ and $q_0 = 0.1$ is assumed.

2 Cosmic star formation history

The star formation properties of the universe at high redshift form one of the focal points of current observational research in cosmology. Recently, our current understanding of the cosmic star formation history has been summarized [16] by combining the local H α objective prism survey results [8] and low redshift ($z < 1$) Canada-France redshift survey (CFRS) results [14] with estimates of the SFD at $z \sim 2.75$ and $z \sim 4$ based on the Hubble Deep Field (HDF) data. These combined data sets indicate a SFD rapidly increasing with cosmic time at high redshift, reaching a maximum at $z \sim 1.5 - 2$ and decreasing at lower redshifts [16]. Semi-analytical models of galaxy evolution in a hierarchically clustering cold dark matter (CDM) universe [1] provide a remarkably good fit to the derived redshift dependence of the SFD.

This scenario provides a very suitable starting point for future research. There are two obvious lines of investigation which urgently need to be pursued and which can be addressed by near-IR emission line surveys.

1. Given the pronounced peak in the SFD between $z \sim 1.5$ and 2, and its remarkable agreement with the peak of the comoving number density of active galactic nuclei (AGNs) at similar redshifts [25] and the peak in the density of damped Ly α absorbers [27], this epoch appears to be of fundamental importance for the formation of present-day galaxies. However, no direct measurements of the SFD in this redshift range are available, and the inferred peak in the SFD follows only from the fact that both from higher and from lower redshifts, the SFD increases as this epoch is approached. Direct measurements of the SFD out to $z \sim 2.5$, i.e., covering the SFD peak era as well as the preceding and following epochs, are therefore crucially important.
2. The SFDs at $z \sim 2.75$ and $z \sim 4$ are based on the rest frame ultraviolet (UV) emission of UV-bright galaxies [16]. Therefore, these points are lower limits, since obscuration by dust will give rise to an underestimate of the derived star formation rates (SFRs) and since UV-obscured star forming galaxies will not be accounted for in the derived SFD. The colours of the HDF objects used to derive the SFD at $z \sim 2.75$ and $z \sim 4$ are similar to those of local UV-selected, but dusty starburst galaxies and inconsistent with an unreddened stellar population. Extinction corrections on the derived high- z SFRs of more than a factor of 10 are derived [18]. Obviously, the uncertainties introduced by

Table 1. Redshift ranges where various bright spectral lines are available in near-IR atmospheric windows.

Line	λ [μm]	Z 0.85 – 0.99 μm	J 1.00 – 1.34 μm	H 1.50 – 1.80 μm	K 2.03 – 2.35 μm
<i>Good star formation tracers</i>					
H α	0.6563	0.30 – 0.51	0.52 – 1.04	1.29 – 1.74	2.09 – 2.58
H β	0.4861	0.75 – 1.04	1.06 – 1.76	2.09 – 2.70	3.18 – 3.83
[O II]	0.3727	1.28 – 1.66	1.68 – 2.60	3.02 – 3.83	4.45 – 5.31
Pa α	1.8751				0.08 – 0.25
<i>Poor star formation tracers</i>					
Ly α	0.1215	6.00 – 7.15	7.23 – 10.0	11.4 – 13.8	15.7 – 18.3
[O III]	0.5007	0.70 – 0.98	1.00 – 1.68	2.00 – 2.60	3.05 – 3.69

the presence of extinction will be strongly alleviated if a star formation tracer at longer wavelength can be used.

Since H α emission is much less strongly affected by dust than shorter wavelength tracers (both in continuum and in spectral lines), and since large format, high quality near-infrared arrays now enable emission-line surveys in the Z , J , H and K -bands, H α surveys will be able to address both of these points, and thus supply unique information on the star formation history of the universe out to $z \approx 2.5$.

3 Use and limitations of H α and other tracers

3.1 Ly α is not a good tracer of star formation

Traditionally, surveys for high- z star forming galaxies have targeted the Ly α line, which moves into the optical regime for $z = 1.9 - 6.0$. However, since Ly α is resonantly scattered, even very small quantities of dust will effectively suppress the line [4, 5, 6]. Indeed, despite painstaking efforts, Ly α surveys have not revealed a population of high- z starburst galaxies [29]. Recent spectroscopic observations of a number of star forming $z > 3$ galaxies selected by the UV dropout technique [26] confirm that Ly α is not a good tracer of star formation in high- z galaxies. These galaxies form stars at rates of $\sim 10 M_{\odot} \text{yr}^{-1}$ as derived from their rest frame UV properties, but Ly α is absent (or in *absorption*) in more than 50% of the cases, while in most of the remaining objects the line is faint [26]. Thus, while Ly α searches can be used to find high- z star forming galaxies [15, 10, 11], such surveys will miss a large fraction of these galaxies, and cannot provide reliable SFRs for the galaxies that are detected.

3.2 H α as a tracer of star formation in galaxies

The problems affecting Ly α surveys are avoided by searching for H α emission instead. The H α line is not resonantly scattered and thus much less sensitive to the effects of small amounts of dust. In addition, the broad-band extinction at H α (6563 Å) is much less than that at Ly α

Table 2. Conversion factors of H α luminosity $L_{\text{H}\alpha}$ into SFR determined for various IMFs and empirically, and into MER, and conversion factors of various other line luminosities into $L_{\text{H}\alpha}$, in the sense Derived = Conversion \cdot Observed.

Derived	Conversion	Observed	Comments
<i>Star formation rate ($M_{\odot} \text{ yr}^{-1}$) from $L_{\text{H}\alpha}$ (L_{\odot})</i>			
SFR	$1.27 \cdot 10^{-8}$	$L_{\text{H}\alpha}$	Salpeter IMF [22]
SFR	$4.06 \cdot 10^{-8}$	$L_{\text{H}\alpha}$	Scalo IMF [23]
SFR	$1.83 \cdot 10^{-8}$	$L_{\text{H}\alpha}$	Miller-Scalo IMF [19]
SFR	$3.41 \cdot 10^{-8}$	$L_{\text{H}\alpha}$	empirical conversion [12]
<i>Metal ejection rate ($M_{\odot} \text{ yr}^{-1}$) from $L_{\text{H}\alpha}$ (L_{\odot})</i>			
MER	$3.25 \cdot 10^{-10}$	$L_{\text{H}\alpha}$	not sensitive to IMF
<i>$L_{\text{H}\alpha}$ (L_{\odot}) from luminosity in other lines (L_{\odot})</i>			
$L_{\text{H}\alpha}$	2.75	$L_{\text{H}\beta}$	sensitive to extinction
$L_{\text{H}\alpha}$	9.71	$L_{\text{Pa}\alpha}$	
$L_{\text{H}\alpha}$	2.22	$L_{[\text{O II}]}$	empirical conversion [13], sensitive to abundance, excitation, IMF and extinction

(1215 Å), $A_{\text{Ly}\alpha}/A_{\text{H}\alpha} = 4.28$ [3]. Hence an H α survey should produce a much more reliable measurement of the SFD of the high- z universe.

In Table 2 the redshift ranges where H α and other lines are available in the near-IR windows are presented. Since the new 1024² Rockwell HgCdTe “Hawaii” arrays still have at least 50% quantum efficiency at wavelengths as short as 0.8 μm , the Z -band (0.85 – 0.99 μm) is included in this table. For H α , the thermal background emission limits sensitive searches to redshifts $z < 2.5$. Near-IR H α surveys thus will be able to fill in the gap between the $z < 1$ results of the CFRS and $z > 2.5$ results of the HDF, and cover the crucial epoch where the SFD in the universe reaches its maximum value.

In interpreting H α observations it is important to take into account that, after correcting for extinction at 6563 Å in the rest frame, and under the usual assumption of case B recombination in ionization bounded, dust-free H II regions, H α measures only the production rate of hydrogen ionizing photons ($\lambda < 912$ Å). Therefore, like the rest frame UV emission, the H α emission measures only the formation rate of *massive* stars, and not directly the total SFR. Hence, H α -derived SFRs are subject to the same uncertainties as UV-derived SFRs as far as the conversion from *massive* SFR to *total* SFR is concerned. This correction involves the *assumption* of an Initial Mass Function (IMF) and is both large and uncertain, as illustrated by Table 3.1. However, like the UV emission, H α emission can be used to reliably measure a *metal ejection rate* (MER), which is dominated by the same massive stars that power the H α emission.

A final uncertainty is introduced by the presence of dust inside the ionized regions. In evolved H II regions such as are found in the disks of quiescent star forming galaxies like the Milky Way, absorption by dust of ionizing photons is unimportant. In (ultra)compact H II regions on the other hand, dust may absorb *most* of the ionizing photons. In Galactic ultra-compact H II regions, at least 50% of the ionizing radiation is absorbed by dust, and in many cases more than 90% [34]. In these cases hydrogen recombination line measurements, even at long wavelengths, will strongly underestimate the Lyman continuum flux of the ionizing sources. In luminous starburst galaxies, and in particular in the more extreme cases such as

the ultraluminous infrared galaxies (ULIRGs), star formation takes place in high density environments and most of the H II regions are compact [35]. As a result, in the objects with the highest SFRs, H α strongly underestimates the SFR. This problem cannot be solved by observing longer wavelength recombination lines, since the line emission is not absorbed but *quenched*, so that *all* nebular emission lines (and the radio free-free continuum) will be suppressed. This phenomenon is found in the prototypical ULIRG Arp 220 [32]. The low Br γ recombination line flux of the nuclei of Arp 220 has been attributed to a very high foreground extinction ($A_V \sim 50^m$) [28]. However, this reasoning fails on the simple grounds that nuclei of Arp 220 are directly detectable in the *J*, *H* and *K*-bands [32], so that the extinction towards the nuclei at these wavelengths must be relatively small. Furthermore, the low radio free-free emission flux density of the nuclei of Arp 220 [24] is unaccounted for in this model. Absorption of ionizing photons by dust in the nuclei of Arp 220 on the other hand naturally accounts for all of these observations [32].

This result has the important implication that shallow H α surveys, probing only the most luminous objects are not suitable for measuring or even constraining the SFD at any redshift. Reliable MERs and SFDs can only be obtained if the luminosity function is probed down to the level where typical local Sc galaxies become detectable, i.e., at rest frame equivalent widths in the H α + [N II] complex $EW_0(\text{H}\alpha + [\text{N II}]) \geq 30 \text{ \AA}$. At this rest frame equivalent width level, the survey depth becomes comparable to the local H α objective prism surveys [9].

3.3 Use and misuse of other lines as star formation tracers

With the exception of Ly α , other hydrogen recombination lines than H α can in principle also be used as star formation tracers. Since the ratios of these lines depend only weakly on physical conditions in the photoionized regions, only extinction plays a role in determining their relative strengths. Unextincted line ratios with respect to H α for the most relevant lines are given in Table 3.1. The only line which can potentially produce *low*-redshift interlopers is Pa α ; at a fixed observing wavelength, all of the other lines sample higher redshifts than H α and thus require much more luminous (and hence rarer) objects to yield detections. Since Pa α interlopers always occur at low *z*, they are relatively easy to recognize. In contrast, optical surveys are strongly plagued by low-*z* interlopers in [O II] and [O III] emission [29]. Nevertheless, in near-IR emission lines surveys it also remains necessary to spectroscopically identify the emission lines in all of the objects detected, since these surveys are sensitive to *any* emission line redshifted to the observing wavelength. This property has often been used to artificially increase the survey volume by simultaneously considering a number of lines, assuming fixed ratios of these lines to H α [17]. However, this procedure is both confusing and dangerous, since ratios of e.g., [O III] 5007 \AA to H α in local galaxies cover large ranges of values [13], and depend strongly on excitation and abundance effects. Other than hydrogen recombination lines, only the [O II] 3727 \AA line is a useable tracer of star formation [13], although it is considerably less well-behaved than the hydrogen lines, and affected by abundance and excitation effects, as well as extinction. More fundamentally, results based on an emission-line survey at a fixed wavelength, but calculated by considering *simultaneously* a number of different lines that can be detected at this wavelength, thus artificially increasing the instantaneous survey volume, completely destroy any information on the redshift dependence of the SFD. The result is a complicated weighted average value over a number of redshifts, and very difficult to interpret. Thus while an emission-line survey at a fixed wavelength can be used to sample simultaneously volumes at a number of different redshifts in different lines (see Table 2), these volumes may not be combined to yield a “redshift-averaged” SFD, but should be treated separately, providing measurements at a number of different redshifts.

4 Narrow-band imaging surveys

Blind emission-line surveys are of three types, probing different regions of parameters space [7]: slitless spectroscopy, long-slit spectroscopy, and narrow-band imaging surveys. Because of the bright background in the near-IR windows, which at $\lambda < 2.2 \mu\text{m}$ is dominated by many narrow airglow emission lines, mainly due to OH, near-IR surveys are best conducted using the narrow-band imaging method. Briefly, this technique consists of deep integration in a narrow-band filter (optimally chosen such that bright airglow lines are avoided) isolating a narrow redshift interval for a given spectral line. Objects showing a narrow-band flux excess when compared to a broad-band image are emission line candidates. Spectroscopic follow-up for securely confirming and identifying the spectral lines and for accurately determining their fluxes, is required. The choice of narrow-band filter width is determined by a trade-off between survey speed (which suffers if the filters are too narrow) and equivalent width sensitivity (which is degraded for filters which are too wide).

4.1 The ESO near-IR $\text{H}\alpha$ survey

Recently, a new survey has been carried out at the ESO/MPI 2.2 m telescope [33]. Based on the considerations of Sect. 3.2 the survey was designed to emphasize depth more than area coverage. For the first time, detections were obtained. A detailed description of the survey parameters and observation and reduction procedures is given elsewhere [33]. The total area covered is $48.0 \text{ } \square'$, and the total comoving volume sampled for $\text{H}\alpha$ emission is $9.0 \cdot 10^3 h_{75}^3 \text{ Mpc}^3$ for $q_0 = 0.1$ (or $3.0 \cdot 10^3 h_{75}^3 \text{ Mpc}^3$ for $q_0 = 0.5$), which is about 50% of the volume of the largest survey to date [31]. However, with an area-weighted 3σ point-source sensitivity of $1.9 \cdot 10^{-16} \text{ erg s}^{-1} \text{ cm}^{-2} \mu\text{m}^{-1}$ in the narrow-band frame, the ESO survey goes considerably deeper. In the entire survey, *two* serendipitous objects were found with a narrow-band excess significant at about the 4σ level.

The limits implied by this survey are presented in Fig. 4, in terms of a comoving number density of galaxies more luminous in $\text{H}\alpha$ than a certain luminosity. The ESO survey produces the best currently available limits for SFRs in the range of 20 to $60 \text{ M}_\odot \text{ yr}^{-1}$. It is significant that the two serendipitously detected objects found in this survey have SFRs in this range. Locally, such SFRs are found in starburst galaxies. It is clear that in the absence of evolution in the $\text{H}\alpha$ luminosity function no detections would be expected in any of the surveys. However, strong evolution is known to take place. Since both $\text{H}\alpha$ and far-infrared (far-IR) emission are proportional to SFR, it is reasonable to assume similar evolution laws for the $\text{H}\alpha$ and far-IR luminosity functions. The evolution of the far-IR luminosity function can be described by pure luminosity evolution $\propto (1+z)^3$, or pure density evolution $\propto (1+z)^{5.8}$ [21]. The local $\text{H}\alpha$ luminosity function, evolved according to these evolutionary scenarios, is plotted in Fig. 4, where we have continued the evolution to a redshift z_e . Inspection of Fig. 4 suggests that many detections would be expected for $z_e = 2$, and a fair number for $z_e = 1$ as well. Since the highest SFRs will be underestimated by $\text{H}\alpha$ (Sect. 3.2), the analysis will be limited to low luminosities. For $z_e = 2$, both luminosity and density evolution of the forms adopted here are ruled out by the ESO survey; in the case of density evolution, the strongest constraint is provided by the small-area Keck survey [20]. For $z_e = 1$, density evolution is fully compatible with all surveys, while luminosity evolution cannot be ruled out given that the $\text{H}\alpha$ emission may be somewhat suppressed at the relevant SFRs. In summary, these results rule out evolutionary scenarios of the types considered here if this evolution continuous backward to $z_e = 2$; however, for $z_e = 1$ the survey limits are not violated. Obviously, the same kind of agreement can be obtained by lowering the exponent of the evolutionary law.

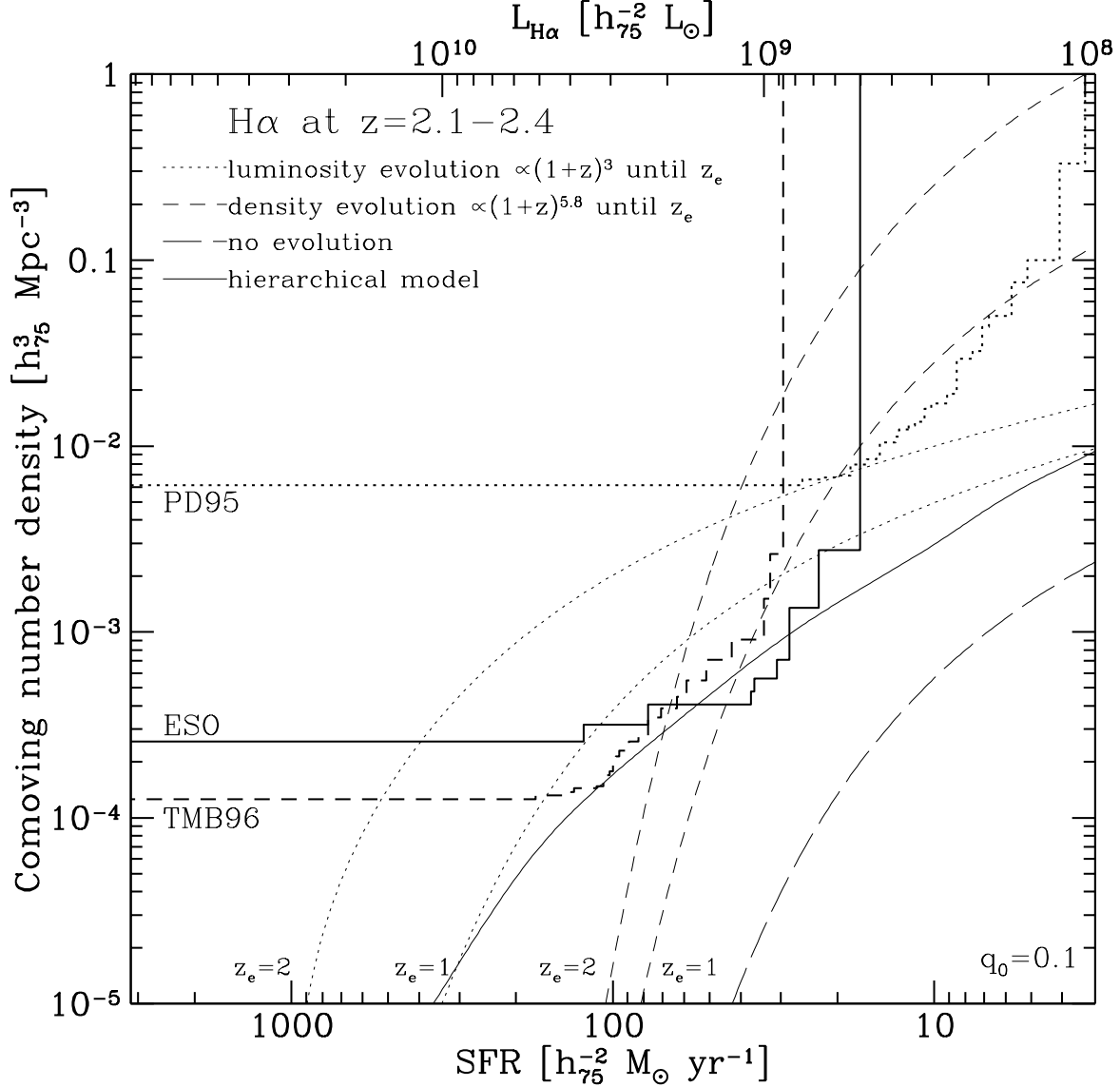


Figure 1. Limits of the ESO near-IR $H\alpha$ survey expressed as limiting comoving number density (vertical axis) of galaxies with $H\alpha$ luminosity (top horizontal axis) or total SFR (bottom horizontal axis) exceeding the values indicated on the horizontal axes. SFRs were calculated assuming the empirical conversion factor [12] (see Table 3.1). The comoving number density limits represent 90% confidence levels based on Poisson statistics. $H\alpha$ luminosity and SFR limits denote 3σ levels. For comparison, the results of two most important earlier surveys [20, 31], reanalyzed in a fashion identical to the ESO survey, and considering *only* $H\alpha$ at $z = 2.1 - 2.4$ are also shown (labeled “PD95” and “TMB96” respectively). The long-dashed curve represents the cumulative local $H\alpha$ luminosity function [8]. The dotted curves show this cumulative luminosity function after applying pure luminosity evolution proportional to $(1+z)^3$ ending at a redshift z_e . Similarly, the short-dashed curves are based on the local $H\alpha$ luminosity function assuming pure density evolution proportional to $(1+z)^{5.8}$ ending at redshift z_e . Evolutionary calculations for both $z_e = 1$ and $z_e = 2$ are shown. The continuous curve is the cumulative $H\alpha$ luminosity function at $z = 2.25$ resulting from a semi-analytical calculation of galaxy formation and evolution in a hierarchically clustering CDM universe [1].

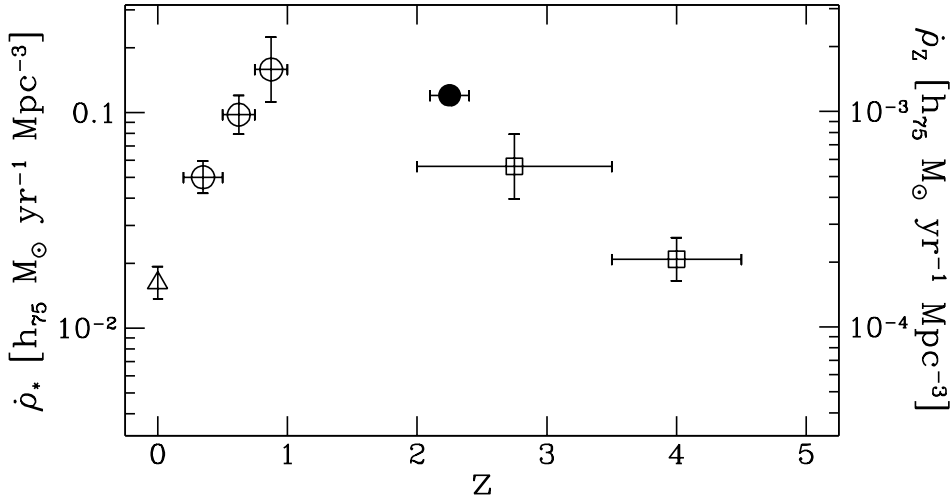


Figure 2. Implications of the $z = 2.25$ results of the ESO near-IR $H\alpha$ survey (filled circle) for the SFD (left vertical axis) and MER (right vertical axis) compared to the rest frame UV-derived values based on the CFRS [14] (open circles) and the HDF [16] (open squares) and the local $H\alpha$ survey [8] (open triangle). The vertical error bar for the ESO $H\alpha$ point has been omitted. Star formation densities were derived from $H\alpha$ luminosity densities using the empirical conversion factor [12]. Points denoted by open symbols were converted to the same scale using the conversion factors in Table 3.1. For reasons discussed in Sect. 2, the UV-derived points (open circles and squares) should be considered lower limits.

A cumulative $H\alpha$ luminosity function for $z = 2.25$, kindly supplied by Carlton Baugh and based on a semi-analytical model of galaxy formation and evolution in a hierarchically clustering CDM universe [1], is also shown in Fig. 4. It is remarkable that this model provides a very good match to the observational results. This model predicts only detections in the ESO survey, with SFRs of $30 - 70 M_{\odot} \text{yr}^{-1}$, in complete agreement with the results. While the number of detections is still very small, it is clear that the ESO survey begins to approach luminosities and volume densities predicted by sophisticated modeling.

4.2 Implications for star formation at $z = 2.25$

Inspection of Fig. 4 shows that only part of the $H\alpha$ luminosity function at $z = 2.25$ is sampled. Hence, a SFD obtained by considering only the detected objects is a firm *lower limit* to the total SFD at $z = 2.25$. Not unexpectedly, the resulting value of $0.014 M_{\odot} \text{yr}^{-1} \text{Mpc}^{-3}$ lies significantly below the value expected based on rest frame UV data [16].

In order to estimate the *total* SFD at $z = 2.25$, the part of the luminosity function not represented in the survey must be accounted for. The detections are quite luminous and, in terms of a Schechter luminosity function, likely significantly brighter than L_* at $z = 2.25$. Consequently, the correction to a total SFD is large, and, since L_* at $z = 2.25$ is not known, uncertain. As noted in Sect. 4.1, the luminosity function for $z = 2.25$ based on the semi-analytical hierarchical model [1] provides the best fit to the available $H\alpha$ data, and also correctly reproduces a number of other observations. In the absence of a direct observational determination, this luminosity function is therefore the best choice for $H\alpha$ emission at $z = 2.25$. Integration of this luminosity

function yields a total comoving SFD at $z = 2.25$ of $0.12 M_{\odot} \text{ yr}^{-1} \text{ Mpc}^{-3}$. As can be seen in Fig. 4.1, this value is in good agreement with the SFD expected based on the analysis by M96. Given the very small number of objects involved, the agreement is very encouraging.

5 Outlook

The above results and considerations lead to two observational recommendations.

1. In order to provide a measurement of the SFD at a particular redshift, near-IR emission line surveys must probe the luminosity function down to sufficiently faint levels. Ideally, such surveys should aim to determine the luminosity function of star forming galaxies at the relevant redshifts directly, removing the need of assuming a luminosity function. The new generation of 8 m class telescopes equipped with large-format near-IR array cameras will provide the required sensitivity and survey power. By carrying out narrow-band searches at a number of discrete redshift intervals, selected to avoid bright airglow lines in the narrow-band filters, near-IR $H\alpha$ surveys will trace the cosmic star formation history out to $z \sim 2.5$, including the important $z = 1.5 - 2$ era where the cosmic star formation density is believed to peak. Higher redshifts will be available by using $H\beta$ or $[O II]$. These surveys will be much less sensitive to uncertainties and biases introduced by extinction than rest frame UV based searches.
2. The brightest part of the galaxy luminosity function cannot be probed using nebular emission line surveys. Here total SFRs must be derived from the rest frame far-IR continuum. At low z , the brightest, optically obscured part of the luminosity function accounts for only a small fraction of the total SFD. However, if strong luminosity evolution takes place, this fraction may become significant at higher redshift. Blind submillimetre surveys (sampling the far-IR continuum of high- z galaxies) are required to address this point observationally. The FIRST mission will play a major role in this field. In the immediate future, a first assessment of the importance of dusty, very luminous star forming galaxies at high z will be made with the SCUBA submillimetre camera at the James Clerk Maxwell Telescope.

Acknowledgements. I am very grateful to Nicolas Cretton for translating the abstract of this review into French, and to Carlton Baugh for supplying the cumulative luminosity function shown in Fig. 4 based on his hierarchical model. Of those involved in the ESO near-IR $H\alpha$ survey, I would like to thank in particular Alan Moorwood and Malcolm Bremer, for their efforts and for ongoing discussion. Finally, I would like to thank the organizers for inviting me to this very enjoyable meeting. The research of Van der Werf has been made possible by a fellowship of the Royal Netherlands Academy of Arts and Sciences.

References

- [1] Baugh, C.M., Cole, S., Frenk, C.S., & Lacey, C.G., 1997, MNRAS, in press
- [2] Bunker, A.J., Warren, S.J., Hewett, P.C., & Clements, D.L. 1995, MNRAS, 273, 513
- [3] Cardelli, J.A., Clayton, G.C., & Mathis, J.S. 1989, ApJ, 345, 245
- [4] Charlot, S., & Fall, S.M. 1991, ApJ, 378, 471

- [5] Charlot, S., & Fall, S.M. 1993, *ApJ*, 415, 580
- [6] Chen, W.L., & Neufeld, D.A. 1994, *ApJ*, 432, 567
- [7] Djorgovski, S., 1992, in: De Carvalho, R.R. (ed.), *Cosmology and large-scale structure in the universe*, ASP Conference Series 24, (San Francisco: Astronomical Society of the Pacific), p. 73
- [8] Gallego, J., Zamorano, J., Aragón-Salamanca, A., & Rego, M. 1995, *ApJ*, 455, L1
- [9] Gallego, J., Zamorano, J., Rego, M., & Vitores, A.G. 1997, *ApJ*, 475, 502
- [10] Giavalisco, M., Steidel, C.C., & Szalay, A. 1994, *ApJ*, 425, L5
- [11] Hu, E.M., McMahon, R.G., & Egami, E. 1996, *ApJ*, 459, L53
- [12] Kennicutt, R.C. 1983, *ApJ*, 272, 54
- [13] Kennicutt, R.C. 1992, *ApJ*, 388, 310
- [14] Lilly, S.J., Le Fèvre, O., Hammer, F., & Crampton, D. 1996, *ApJ*, 460, L1
- [15] Macchetto, F., Lipari, S., Giavalisco, M., Turnshek, D.A., & Sparks, W.B. 1993, *ApJ*, 404, 511
- [16] Madau, P., Henry C. Ferguson, Dickinson, M.E., Giavalisco, M., Steidel, C.C., & Fruchter, A. 1996, *MNRAS*, 283, 1388
- [17] Mannucci, F., & Beckwith, S.V.W. 1995, *ApJ*, 442, 569
- [18] Meurer, G.R., Heckman, T.M., Lehnert, M.D., Leitherer, C., & Lowenthal, J., 1997, *ApJ*, in press
- [19] Miller, G.E., & Scalo, J.M. 1979, *ApJS*, 41, 513
- [20] Pahre, M.A., & Djorgovski, S.G. 1995, *ApJ*, 449, L1
- [21] Rowan-Robinson, M., 1996, in: Bremer, M.N., Van der Werf, P.P., Röttgering, H.J.A., & Carilli, C.L. (eds.), *Cold gas at high redshift*, (Dordrecht: Kluwer), p. 61
- [22] Salpeter, E.E. 1955, *ApJ*, 121, 61
- [23] Scalo, J.M. 1986, *Fund. Cosm. Phys.*, 11, 1
- [24] Scoville, N.Z., Sargent, A.I., Sanders, D.B., & Soifer, B.T. 1991, *ApJ*, 366, L5
- [25] Shaver, P.A., Wall, J.V., Kellermann, K.I., Jackson, C.A., & Hawkins, M.R.S. 1996, *Nat*, 384, 439
- [26] Steidel, C.C., Giavalisco, M., Pettini, M., Dickinson, M., & Adelberger, K.L. 1996, *ApJ*, 462, L17
- [27] Storrie-Lombardi, L.J., McMahon, R.G., & Irwin, M.J. 1996, *MNRAS*, 283, L79
- [28] Sturm, E., et al. 1996, *A&A*, 315, L133
- [29] Thompson, D., & Djorgovski, S.G. 1995, *AJ*, 110, 982
- [30] Thompson, D., Djorgovski, S., & Beckwith, S.V.W. 1994, *AJ*, 107, 1
- [31] Thompson, D., Mannucci, F., & Beckwith, S.V.W. 1996, *AJ*, 112, 1794
- [32] Van der Werf, P.P., & Israel, F.P., 1997, in preparation
- [33] Van der Werf, P.P., Bremer, M.N., Moorwood, A.F.M., Röttgering, H.J.A., & Miley, G.K., 1997, in preparation
- [34] Wood, D.O.S., & Churchwell, E. 1989, *ApJS*, 69, 831
- [35] Zhao, J.H., Anantharamaiah, K.R., Goss, W.M., & Viallefond, F. 1997, *ApJ*, 482, 186